Experimental Characterization of a Chip-Level 3-D Printed Microjet Liquid Impingement Cooler for High-Performance Systems

Tiwei Wei, *Member, IEEE*, Herman Oprins, *Member, IEEE*, Vladimir Cherman, *Associate Member, IEEE*, Shoufeng Yang, Ingrid De Wolf, *Senior Member, IEEE*, Eric Beyne, *Senior Member, IEEE*, and Martine Baelmans

***Abstract*— The chip-level bare die direct liquid impingement jet cooling is regarded as a highly efficient cooling solution for high-performance applications. Furthermore, it shows potential to be integrated inside the chip package. In previous studies, we demonstrated this cooling concept using a prototype fabricated with mechanical micromachining using polymers. With the improvement of fabrication resolution, additive manufacturing or 3-D printing technology enables the fabrication of low-cost polymer microjet coolers with complex internal 3-D geometries and allows easy customization of the cooler design. In this paper, a chip-level impingement jet cooler with a 4 × 4 jet array and 575-μm nozzle diameter is fabricated with high-resolution stereolithography, and assembled directly on the top of the bare die. The modeling study shows that the pressure drop in the 3-D printed cooler is reduced by 24% compared to the micromachined (MM) cooler with the same nozzle dimensions thanks to an improved more complex internal geometry. The fabrication quality and tolerances of the printed cooler are evaluated using optical measurements, scanning acoustic microscope (SAM) inspection, and cross-sectional analysis, showing a measured average nozzle diameter of 575 μm compared to the designed nozzle diameter of 600 μm. Moreover, the 3-D computational fluid dynamics (CFD) simulations used in this paper are experimentally validated by chip temperature measurements. The achieved minimal thermal resistance of 3-D printed 4 × 4 cooler is 0.16 cm^2·K/W for a flow rate of 1000 mL/min. The benchmarking study shows the cooler size can be reduced by a factor of 6.5 by using the 3-D printing technology compared to the MM cooler.**

***Index Terms*— 3-D printing, chip level, computational fluid dynamics (CFD), direct cooling, impingement jet.**

Manuscript received December 3, 2018; revised February 11, 2019 and March 12, 2019; accepted March 13, 2019. Date of publication March 18, 2019; date of current version September 26, 2019. This work was supported in part by the imec Industrial Affiliation Program on 3-D System Integration, in part by the imec Partners, and in part by the imec Reliability, Electrical Testing, Modeling, and 3-D Technology teams. Recommended for publication by Associate Editor J. Weibel upon evaluation of reviewers' comments. *(Corresponding author: Tiwei Wei.)*

T. Wei is with the Department of Mechanical Engineering, KU Leuven, 3001 Leuven, Belgium, and also with imec, 3001 Leuven, Belgium (e-mail: tiwei.wei@imec.be).

H. Oprins, V. Cherman, and E. Beyne are with imec, 3001 Leuven, Belgium (e-mail: Herman.Oprins@imec.be; Vladimir.Cherman@imec.be; Eric.Beyne@imec.be).

S. Yang and M. Baelmans are with the Department of Mechanical Engineering, KU Leuven, 3001 Leuven, Belgium (e-mail: shoufeng.yang@kuleuven.be; martine.baelmans@kuleuven.be).

I. De Wolf is with the Department of Materials Engineering, KU Leuven, 3001 Leuven, Belgium, and also with imec, 3001 Leuven, Belgium (e-mail: Ingrid.DeWolf@imec.be).

Color versions of one or more of the figures in this article are available online at http://ieeexplore.ieee.org.

Digital Object Identifier 10.1109/TCPMT.2019.2905610

I. Introduction

With the increasing demand of the heat flux on high-performance electronic applications, the thermal management becomes more and more challenging, especially for 3-D integrated systems [1]. The bare die liquid jet impingement cooling is an efficient cooling technique that has been successfully applied using several fabrication techniques including Si deep reactive-ion etching (DRIE) microfabrication [2], multilayer ceramic technology (MLC) [3], and fabrication methods for metal [4], [5]. Whereas the Si, ceramic, and metal coolers involve expensive fabrication techniques, cooling solution using low-cost fabrication methods become a promising trend for industry applications. In [6], we have introduced a chip-level 3-D-shaped polymer cooler fabricated using mechanical micromachining for a 4×4 nozzle array with 600-μm-diameter nozzles. The multijet cooler can achieve heat transfer coefficients up to 6.25×10^4 W/m^2·K with a pump power as low as 0.3 W. The results show that cost-efficient polymer-based fabrication can be used to create a high-performance chip-level cooler with submillimeter nozzle diameters. This fabrication method, however, requires different individual parts to be fabricated separately and then assembled together. Furthermore, it limits the design of the cooler to simple, straight geometries that can be fabricated using micromachining.

In recent years, the 3-D printing or additive manufacturing has become an emerging fabrication technique in electronic packaging [7]–[10] by providing the opportunities of embedded electronic component in a single module, multiple materials printing, and 3-D packages geometry with circuitry and components printing [11]. Typical 3-D printing methods include: 1) stereolithography (SLA); 2) fused deposition modeling (FDM); 3) selective laser sintering; and 4) inkjet printing [12]. SLA uses either galvo scanners to guide the UV lasers or projectors to cure photopolymers layer by layer. Typically, the fabrication tolerance is limited to a few hundreds of micrometers in the commercial systems and further development is required to fabricate more performant coolers. In research tools, smaller feature sizes are possible since the resolution depends on the size of the printing platform with fixed number of pixels. Tehrani *et al.* [13] demonstrated a series of "smart" microelectronic packages by utilizing fully additive inkjet and 3-D printing fabrication technologies,

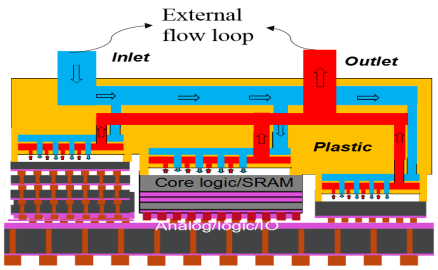

Fig. 1. Schematic of the application of a customizable 3-D printed cooler on a high-performance 3-D module.

which includes 3-D square encapsulants, microfluidic channels, and through-mold-via (TMV) interconnects. Goubault *et al.* [14] built encapsulation packages and lids onto the silicon substrate using the SLA technology.

The 3-D printing technology also has great potential for the application of electronics cooling solutions. The main advantage of additive manufacturing is that it can use low-cost materials for the cooler fabrication and to print the whole geometry in one piece, while creating complex internal geometries. It was first introduced for the fabrication of the complex shapes obtained from topology optimization of air-cooled heat sinks [15] and later for more advanced liquid cooling solutions such as microchannel heat sinks [16] and impingement coolers [17], [18]. Jenkins *et al.* [17] demonstrated an aluminum alloy ($AlSi_{10}Mg$) microchannel heat sink with straight, parallel channels by using the direct metal laser sintering (DMLS) process, where inlet nozzle diameter is 500 μm. The fabrication of impingement coolers has been demonstrated for coolers with a common return and with relatively large nozzle diameters of 1 mm for metal using laser sintered 3-D printing technology [18] and UV curable acrylic plastic using SLA [19]. Robinson *et al.* [18] demonstrated a high-efficiency microjet array cooler using a micrometal additive manufacturing process with 30-μm-diameter nozzles. However, metal-based bare die cooling solutions are expensive and have a high risk for the device reliability due to introduction of metal (Cu and Al) in very large scale integration (VLSI) devices.

In this paper, we present the concept, design, fabrication, and experimental characterization of a cost-efficient 3-D printed polymer-based chip-level liquid impingement cooler with submillimeter-diameter nozzles and with distributed outlet channels in between the inlet channels, targeted to directly cool the backside of high-performance chips, 3-D chip stacks, or interposer-based packages (Fig. 1). The chip-level cooler is part of a closed-loop cooling circuit that includes an external pump, the tubing, and a heat exchanger used to cool the heated up liquid coolant back to the initial temperature. For an assessment of the cooling efficiency of the application, the overall thermal performance of the full loop should be evaluated. However, the focus of this paper is on the thermal performance of the cooler itself, in terms of the temperature difference between the junction of the chip and the coolant inlet temperature, and the pressure drop in the cooler. The characterization of the cooler enables the relative performance comparison of different coolers in the same closed-loop liquid cooling circuit.

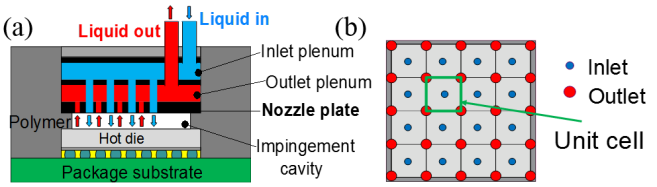

Fig. 2. Chip-level impingement cooler concept. (a) Schematic of multijet cooler. (b) Top view of the nozzle plate with jets array [6].

In order to evaluate the thermal performance, the fabricated 3-D-shaped polymer cooler is assembled to our 8 mm $\times$ 8 mm thermal test chip [20] with integrated heaters and temperature sensors. First, the concept and the design of the impingement cooler with a 4×4 inlet nozzle array and the design limitations related to the fabrication tolerances are discussed in Section II. Next, in Section III, an analysis of the tolerances of the fabricated coolers is presented, and a new defect detection metrology based on the scanning acoustic microscope (SAM) measurements is introduced to detect defects inside the printed cooler. In Section IV, the experimental thermal and hydraulic characterization of the fabricated cooler are discussed. In Section V, the thermal performance of the printed cooler is benchmarked with the performance of a conventional air cooling heat sink and of the micromachined (MM) cooler [6].

II. Design of 3-D Printed Microjets Cooler

A. 3-D Printing Constraints and Cooler Critical Design Parameters

In this paper, the designed cooler is printed using the SLA process. For the SLA process flow, the designed 3-D printed cooler computer-aided design (CAD) structure is first broken down by a series of points and lines using Fusion 360 design software. Then, a laser beam with certain laser spot size moves across the print area, and the photopolymer resins are solidified as it goes along. Therefore, the resolution of the SLA process is determined by the laser spot size. For the used SLA 3-D printer, the resolution for the first layer thickness is 0.05 mm. The minimum feature size is 0.13 mm for the *xy* plane and 0.406 mm for the *Z* build direction, respectively. To ensure the structural integrity, special support structures with finer dimensions are built inside the internal geometry, such as thick cavity or channels.

The concept of the bare die chip-level impingement jet cooler is shown in Fig. 2. Fig. 2(a) shows the cross section of the multijet cooler with a 4×4 array of inlet nozzles and a 5×5 array of outlet nozzles distributed in between the inlets, shown in the top view of Fig. 2(b). Fig. 2(b) reveals four critical layers: inlet plenum, outlet plenum, nozzle plate, and impingement cavity layer. The inlet plenum is used as the flow distributor to distribute the cold water inside the 4×4 inlet nozzles. After the fluid impinged onto the chip backside, the outlet plenum is used as flow collector for the flow from the 5×5 outlet nozzles. As shown in Fig. 3(a), the geometrical design of the 3-D printed microjet cooler should take into account the manufacturability of the SLA printer including printing resolutions and laser spot size. The nozzle diameter d_i and the nozzle plate thickness t are the

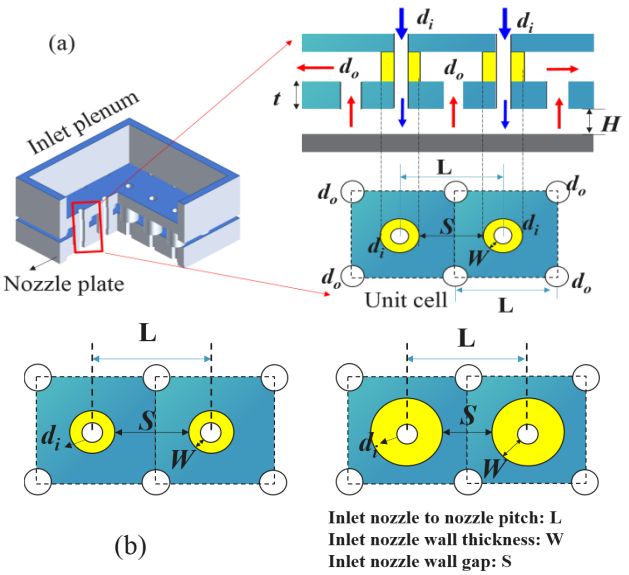

Fig. 3. Design consideration. (a) Critical design parameters limitations for the use of 3-D printing for impingement coolers. (b) Indication of the impact of wall thickness on the gap S in the outlet plenum between adjacent inlet nozzles.

critical dimensions since they determine whether the excess liquid resin can be removed sufficiently through the tiny nozzle channels. Moreover, the nozzle wall thickness W used as the separation between the inlet nozzle and the outlet plenum should be strong enough to withstand high flow pressure and prevent leakage.

As shown in Fig. 3(b), the gap S between the external walls of two adjacent inlet nozzles in the outlet plenum is also very important. In this outlet plenum layer, the walls of the inlet nozzles, which go vertically through this layer, act as a divider between the (vertical) inlet flow and the (horizontal) outlet flow. By decreasing the gap S (for a fixed nozzle pitch and internal diameter, thus by increasing the wall thickness W), the available area for the coolant to flow in the horizontal outlet plenum reduces. Since the pitch and internal diameter do not change, there is no impact on the pressure drop for the vertical direction through the nozzles. However, the pressure drop in the outlet plenum where the coolant flows through the inlet/outlet dividers increases as the nozzle wall thickness W becomes thicker for a fixed nozzle pitch.

Other design parameters such as tube connections, cavity height H, and the O-ring groove are also taken into account for a better design. The inlet connection is designed in the center of the cooler in order to improve the flow distribution over different inlet nozzles. The rest of the available space in the cooler material can be used to improve the outlet chamber design to help the outlet flow evacuation. In [2], the impact of the cavity height H variation on the cooler thermal/hydraulic performance was investigated. It shows that the heat transfer coefficient and the pressure drop are inversely proportional to the gap height in the pinchoff regime at gaps $H < H_{\text{critical}}$ while the heat-transfer coefficient is constant in the impingement regime with $H \geq 1.2D_{\text{in}}$. For practical considerations, the cavity height chosen in this paper is 0.6 mm in the impingement regime, where no significant impact on the heat-transfer coefficient is observed.

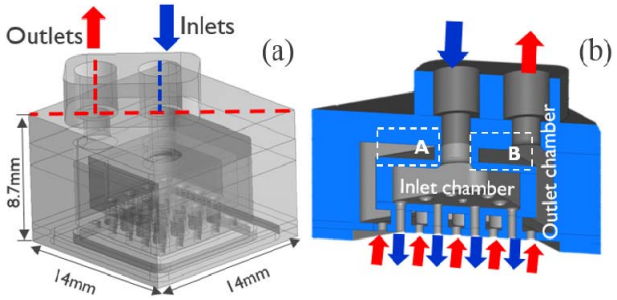

Fig. 4. CAD structure of 3-D printed 4 × 4 cooler. (a) Transparent view. (b) Cross-sectional view.

TABLE I
GEOMETRY COMPARISON BETWEEN MM COOLER AND 3-D PRINTED COOLER

Geometry		MM cooler	3D printed Cooler
Nozzle array	N	4×4	4×4
Inlet chamber height		3 mm	2.5 mm
Inlet diameter	d_i	0.6 mm	0.6 mm
Outlet diameter	d_o	0.6 mm	0.6 mm
Cavity height	H	0.6 mm	0.6 mm
Nozzle plate thickness		3 mm	0.55 mm
Cooler size	x,y,z	46×46×13 (mm^3)	18×18×8.7 (mm^3)

B. Printed Cooler Design

The proposed design of the 4×4 inlet jet array cooler with 600-μm-diameter nozzles for the 8 mm × 8 mm thermal test chip on the 14×14 mm^2 package substrate is shown in Fig. 4. This design takes into account the manufacturability aspects of the used 3-D printer as well as the critical design parameters described above. The cavity height H is 600 μm, while the wall thickness of the nozzles W and the gap between two nozzles in the outlet plenum S are both 400 μm. Since the flow maldistribution is an important aspect for multijet impingement cooling, several computational fluid dynamics (CFD) studies on the impact of the inlet plenum dimensions have been performed to improve the flow distribution uniformity [21]. The results show that a lower plenum height can generate more flow maldistributions, with higher velocity concentrating in the nozzles in the center of the cooler. The inlet diameter and plenum height both should be considered when designing the impingement cooler. Therefore, the inlet chamber thickness is chosen as 2.5 mm, based on the tradeoff between the cooler size and flow distributions. Moreover, both in the inlet chamber and the top part of the outlet chamber, support pillars have been added to ensure the structural integrity. The geometric dimensions comparison between the MM cooler and 3-D printed cooler are summarized in Table I.

Fig. 5 shows the internal structure of the MM cooler [6] and the 3-D printed cooler side by side. In general, the process flow of the 3-D printed cooler is simple since all the parts can be printed in a whole as a single part while creating the complex 3-D geometries including cavities and O-ring grooves. For the MM cooler, all the individual parts have to be fabricated separately and glued together, which might cause a higher risk of water leakage. Furthermore, the jet nozzles must be

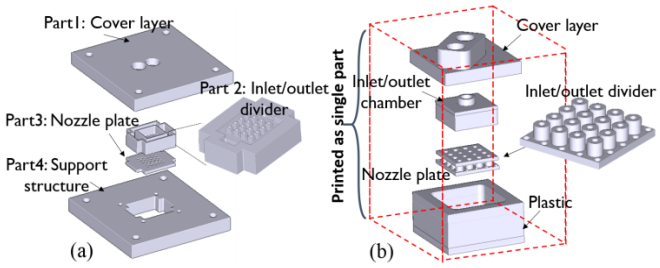

Fig. 5. Internal CAD structures comparison between (a) mechanical MM cooler [6] and (b) 3-D printed cooler.

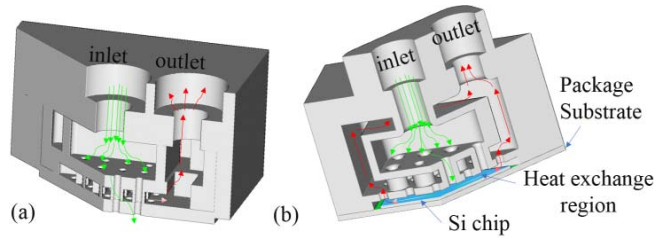

Fig. 6. Cooler structure with the pressure reduction of shape optimization. (a) MM cooler. (b) 3-D printed cooler.

drilled by microdrilling, where the nozzle diameter is limited by the mill tool diameter. As indicated in Fig. 5(b), inlet and outlet dividers can be printed as hollow cylinders to separate the inlet flow and outlet flow, which can significantly reduce the pressure drop compared to square-shaped dividers shown in Fig. 5(a). In summary, compared to the micromachining prototype, the 3-D printed cooler has a lower fabrication cost, a more flexible and customizable design, and a finer resolution of the internal structures.

Fig. 6 shows a cross section of the printed cooler to visualize the flow inside the internal structure. It can be seen that, by the use of 3-D printing technology, more outlet chamber space can be designed in order to improve the evacuation of the outlet flow at a reduced pressure drop.

C. Modeling Study: Micromachined and Printed Cooler Comparison

In order to evaluate and compare the thermal and hydraulic performance of the two coolers with different fabrication techniques, CFD modeling is used during the initial design stage. The software package used for the CFD study is ANSYS Fluent. Since the thermal performance of the cooler scales with the chip area, the thermal resistance is normalized as follows:

$$R_{\text{th}} = A \cdot (T_{\text{avg}} - T_{\text{in}})/(Q_{\text{heater}}) \tag{1}$$

where T_{avg} is the averaged chip temperature, A is the thermal test chip area, T_{in} is the coolant inlet temperature, and Q_{heater} is the heat generated in the heater cells based on the measured electrical current and heater voltage. The pressure drop is defined as the pressure difference between inlet pressure and outlet pressure

$$\Delta P_{\text{total}} = P_{\text{in}} - P_{\text{out}}. \tag{2}$$

The meshing details of CFD models based on MM cooler and 3-D printed cooler are both shown in Fig. 7. It should be

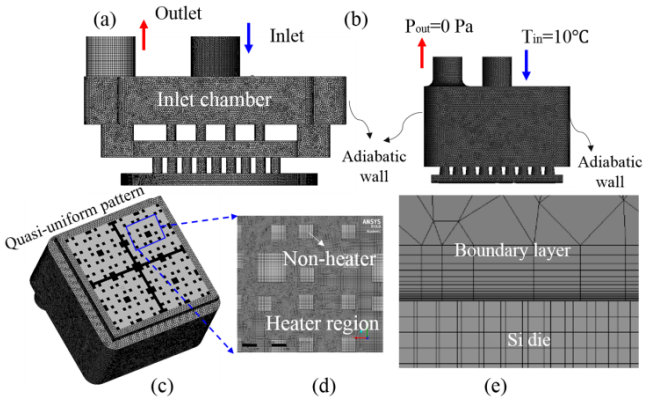

Fig. 7. CFD models with meshing for the comparison of the MM and 3-D printed coolers. (a) MM cooler model. (b) 3-D printed cooler. (c) Bottom view of the 3-D printed cooler model mesh with quasi-uniform heater cells in the test chip. (d) Detailed view of the heater cell meshing. (e) Boundary layer meshing.

noted that Fig. 7(a) and (b) are shown in the same scale, highlighting the compact design of the printed cooler. An adiabatic wall is assumed for the CFD cooler model. We assume that there is no heat loss through the plastic material of the cooler due to the low thermal conductivity. Previous simulations [22] have shown that there is no significant difference for the chip temperature between the model with a fully modeled cooler with low-conductivity material and the model where only the fluidic channels without cooler where considered.

Based on the mesh sensitivity study, the number of elements for the MM cooler demonstrator and for the 3-D printed cooler is 6 million and 4 million, respectively. The first-layer thickness of tetrahedral boundary layer is set as $1e^{-3}$ mm with maximum of 15 layers in order to keep $Y^+ < 1$. The convergence criteria for continuity, x, y, and z velocity is $1e^{-5}$, while the convergence criteria are $1e^{-6}$ for the energy equation. The Re numbers based on the nozzle diameter considered in this paper are in the range from 10 to 3500. The reported range for the turbulent transition for liquid jet impingement flow is from 1000 to 3000 [23]. At the maximum considered flow rate, the flow inside the cooler is therefore slightly turbulent or in the transitional regime. Therefore, the transition shear stress transport (SST) model [23] has been chosen as the turbulence model. The liquid used in this paper is deionized (DI) water, and the inlet temperature is kept at 10 °C. For both cases, the chip power is 50 W with the chip heated area of $8 \times 8 \times 75\%$ mm^2. The details about the chip and its heating elements are shown in Fig. 15 in Section IV.

Fig. 8 shows the pressure distribution results from the full-cooler-level simulations for both coolers. The comparison shows a significantly lower pressure drop for the printed cooler. Exploiting the capabilities of 3-D printing to design the internal cooler geometry results in a reduction of the pressure drop by 24% compared to the geometry of MM cooler [6].

It should be noted that the main reason for the pressure reduction is the difference in internal geometry. As shown in Table I, the critical nozzle parameters are the same for both coolers (at least the nominal design values): inlet/outlet nozzle diameters, cavity height, and nozzle array. However, other parameters are different (nozzle plate thickness,

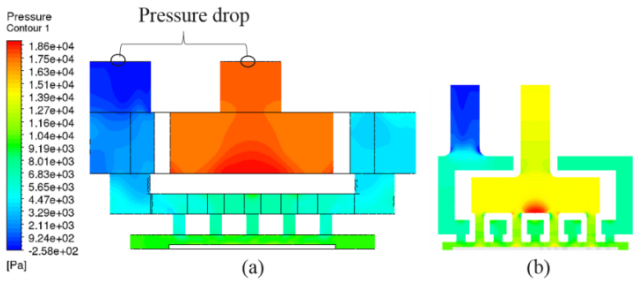

Fig. 8. Pressure comparison between MM and printed cooler for a flow rate of 650 mL/min drawn on the same scale. (a) MM cooler with pressure drop $\Delta P_{\text{total}} = 0.18$ bar. (b) 3-D printed cooler with pressure drop $\Delta P_{\text{total}} = 0.15$ bar.

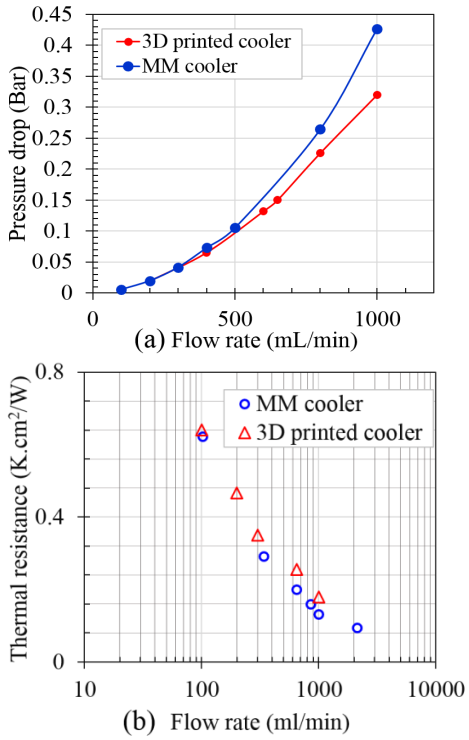

Fig. 9. Comparison between the MM cooler and 3-D printed cooler based on the modeling study. (a) Pressure drop comparison as a function of flow rate. (b) Thermal resistance comparison.

outlet chamber, and inlet chamber). These values are linked to the fabrication capabilities, and therefore, they are inherently part of the comparison. Other aspects that contribute to the pressure reduction are the cylindrical shape of the inlet/outlet (less pressure drop) and rounded inlet/outlet nozzle transitions from/to the plenum. The 3-D printing allows making those features with less pressure drop compared with the MM demonstrator.

In Fig. 9, the thermal resistance and pressure drop as function of flow rate are compared for the MM cooler and 3-D printed cooler. The general trends show that the pressure drop can be reduced for using 3-D printed cooler, while the thermal resistance is similar due to the same design of the nozzle plate.

III. Fabrication Tolerance Analysis

The polymer 3-D printed demonstrator of the jet impingement cooler was printed using SLA with a reported minimal

TABLE II
Material Properties of 3-D Printed Cooler

Material properties	Water absorption	Tg (ºC)	HDT@0.48MPa HDT@ 1.81MPa	CTE ppm/K	Dielectric constant
Watershed	0.35%	39 –46	45.9 - 54.5ºC 49.0 - 49.7ºC	90 - 96	3.9 - 4.1 (60HZ)

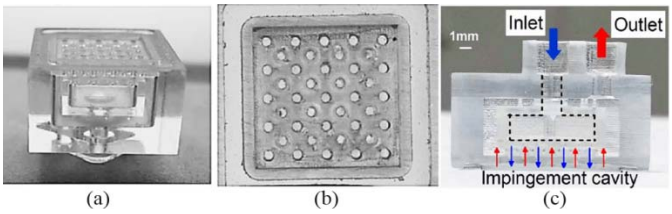

Fig. 10. Demonstration of the 3-D printed cooler. (a) Photograph of the 3-D printed cooler. (b) Bottom view of the nozzle plate with inlet/outlet nozzles. (c) Detail of the channels in cross section of the cooler.

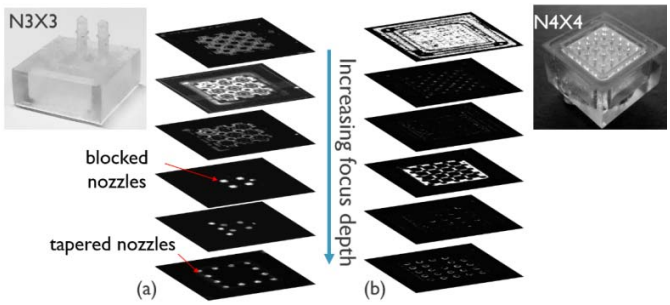

Fig. 11. Defect measurements of the 3-D printed coolers using SAM inspection. (a) Printed cooler with blocked nozzles and tapered nozzles. (b) Printed cooler without blocked nozzles.

feature size of 130 μm and with 50-μm layer thickness. The chosen polymer material, Somos WaterShed XC, is a water-resistant material, which shows ABS-like properties and good temperature resistance. The material properties of the 3-D printed cooler are listed in Table II. The printed demonstrator is shown in Fig. 10. The bottom view of the nozzle plate with inlet/outlet nozzles shows that all the holes are printed uniformly across the cooler. The cross-sectional analysis of the printed 14×14 mm^2 cooler confirmed the successful printing of the cooler and its internal structure and revealed no leftover resin residuals.

Since the 3-D printed cooler is printed as a single part, it is difficult to check for potential internal blockages with residual uncured resin. For this application, we demonstrated that the SAM technique can be used to evaluate the cooler quality. SAM is a nondestructive technique used for microinspection [24]. By adapting the focus depth, the potentially blocked resin inside the nozzles can be detected at different layers in the structure. Fig. 11 shows the two examples of the SAM analysis of a printed cooler with or without defects: From the SAM images, it is possible to differentiate between the open nozzles without resin residues (A), open nozzles with tapered edges (B), and the presence of blocked nozzles (C). Fig. 11(a) shows 3×3 cooler with blocked nozzles and tapered nozzles, while Fig. 10(b) shows 4×4 cooler without defects.

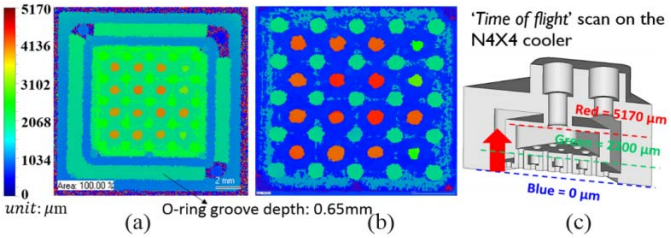

Fig. 12. SAM measurement for assessing the depth of the printed nozzles. (a) SAM image with focused depth on cooler bottom layer and (b) nozzle plate layer. (c) Indication of the depth of different layers.

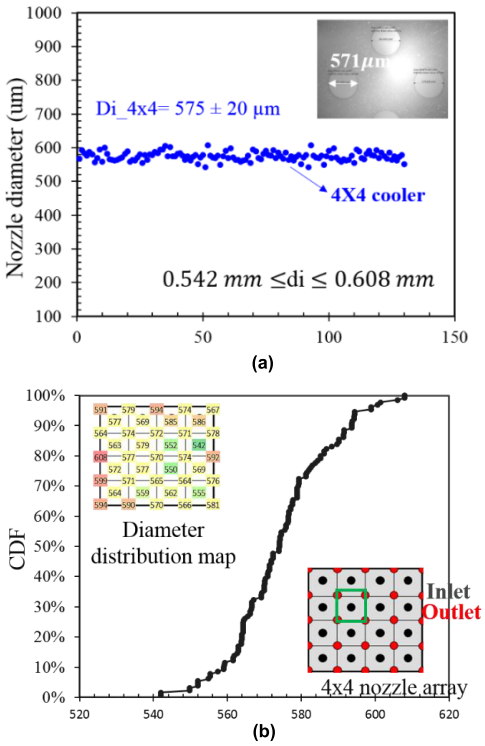

Fig. 13. Evaluation of the fabricated nozzle diameter. (a) Nozzle diameter variation measurements with 4 × 4 cooler. (b) Normal distributions of inlet/outlet nozzle diameters.

"Time-of-flight" scan on the cooler from the bottom side of the cooler can be used to assess the depth of the nozzles inside the cooler from the cooler plot. As shown in Fig. 12, the blue is set as the reference depth as 0 μm. The green indicates depth level of 2.2 mm, while the red represents the height level as 5.1 mm, corresponding to the top surface of the inlet and outlet chambers, respectively.

First, the actual diameter values of the printed inlet and outlet nozzles are measured and analyzed in Fig. 13. The distribution of the nozzle diameter shows that the average nozzle diameter of 130 measured nozzles is 575 μm, which is 5% smaller than the nominal design value of 600 μm. The impact of the nozzle diameter variation on the achieved thermal resistance will be evaluated in Section IV-A, with the comparison between experimental and modeling data.

In the second step of the fabrication assessment, specific geometry details are compared between the fabricated cooler and the designed geometry. As indicated in Fig. 14, four different regions are marked, including inlet nozzle opening,

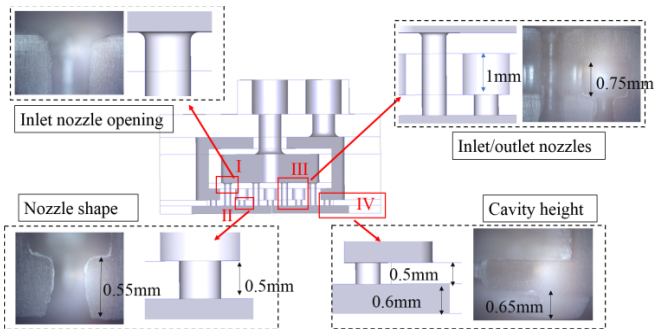

Fig. 14. Comparison between the nominal design and the fabricated 4 × 4 jet array cooler at four different locations.

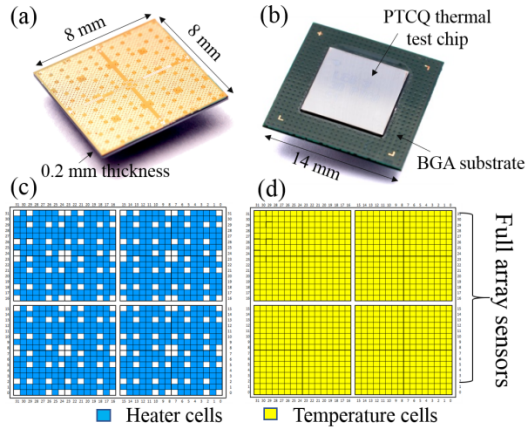

Fig. 15. Detail of the PTCQ thermal test chip. (a) Overview of the thermal test chip patterns. (b) PTCQ BGA package. (c) Configurations of 832 programmable heater cells. (d) Configurations of 32 × 32 array diode temperature sensors.

nozzle plate, inlet/outlet nozzles, and cavity height. After the postcure process, the designed straight corners are rounded due to polymer shrinkage. The angled nozzle walls and the rounded corners of the nozzles will have an impact on the flow distribution, the chip temperature profile, and the pressure drop. The details of this impact will be shown in the modeling session. From the cross section, it can furthermore be observed that the nozzle plate is 0.55 mm compared to the design value of 0.5 mm. (The printed layers are 50 μm thickness.) For the cavity height, the actual height is about 0.65 mm compared to the nominal design value of 0.6 mm.

Finally, the surface roughness of the groove surface is a crucial factor for the sealing ability with the sealing ring. For the early additive manufacturing technologies, the surface roughness is quite high due to the low resolution of the 3-D printing machine. The 3-D printing technology used in this paper is SLA with 50 μm layer thickness. The roughness is expected to be smaller than a layer thickness. The designed groove has a depth of 600 μm. The SAM depth measurement from the cooler's bottom side in Fig. 12 shows a smooth groove surface as an indication of limited roughness.

IV. Thermal and Hydraulic Characterization

The thermal performance of the cooler is evaluated using the thermal test chip PTCQ [20] (Packaging Test Chip version Q), shown in Fig. 15. This 8 mm × 8 mm thermal test chip with

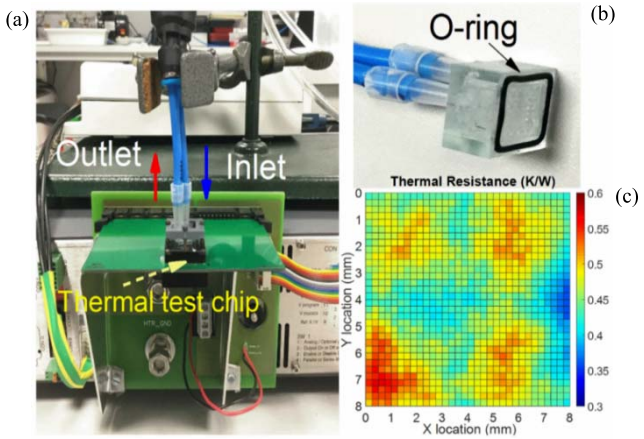

Fig. 16. Experimental setup for the cooler characterization. (a) Assembly of the cooler on the test chip package and PCB. (b) O-ring used for sealing of the cooler on the package substrate. (c) Temperature map measurement for the 3-D printed cooler for a flow rate of 600 mL/min.

array of 32 × 32 temperature sensors and programmable heat dissipation patterns is used for the thermal characterization, allowing detailed chip temperature map measurements. Resistors used as heater cells shown in Fig. 15(c) are fabricated by back-end-of-line (BEOL) processing technology [20]. The single heater cell is equipped with two 200 × 100-μm^2 metal meander heaters. Due to the periphery circuits and the cells with mechanical stress sensors (192 white square elements in Fig. 15(c), the "heater cells" result in a quasi-uniform power dissipation with 75% coverage of the thermal test chip. All the cells in the 32 × 32 array contain diodes as temperature sensors, fabricated by front-end-of-line (FEOL) semiconductor processing, allowing the measurement of the full-chip temperature map, as indicated in Fig. 15(d). The voltage drop across the diode for a constant current is used as the temperature sensitive parameter of the sensor. The calibrated sensitivity is -1.55 ± 0.02 mV/°C for a current of 5 μA in the temperature range between 10 °C and 75 °C.

The cooler and the package are placed in a measurement socket on the PCB and held together by screws. An O-ring is placed in the foreseen groove at the bottom of 3-D printed cooler to create a sealing between the cooler and the package, as shown in Fig. 16. The thermal experiments are performed using DI water as a coolant and for 50 W as quasi-uniform power dissipation in the 8 mm × 8 mm chip area, according to the heater map in Fig. 7(c). The reliable water-resistant polymer material allows performing 48-h measurement without observing cooler deformations or leaks. The thermal measurements with a quasi-uniform power dissipation in Fig. 16 show a low-average thermal resistance of 0.45 K/W (or 0.29 cm^2·K/W) at a flow rate of 600 mL/min and a good temperature uniformity compared to a single jet cooler [6]. In Sections IV-A and IV-B, the thermal and hydraulic performance of the printed cooler are characterized and analyzed for different flow rates ranging from 100 to 1000 mL/min.

A. Thermal Characterization

As shown in Fig. 17(a), the normalized temperature profile along the chip diagonal is plot for different flow rates ranging from 100 to 1000 L/min for the heater pattern of Fig. 7(c).

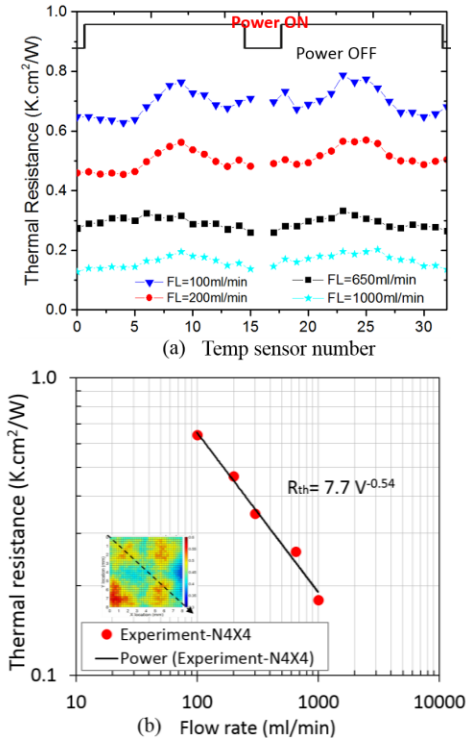

Fig. 17. Thermal characterization of the 3-D printed cooler. (a) Measured temperature profile under different flow rates. (b) Validation of predicted model based on corrected nozzle diameter.

The measurements show that the cooling performance as well as the temperature uniformity across the chip surface improves for increasing flow rate. Due to the high cooling rate of the multijet cooler, the measured temperature profile reveals the pattern of the heated and nonheated cells in the thermal test chip. The relation between the thermal resistance based on the average chip temperature and the total inlet flow rate is also shown in Fig. 17(b). It can be seen that the thermal resistance R_{th} scales with flow rate $\dot{V}$ according to the following power law behavior $R_{\text{th}} \propto \dot{V}^{-0.54}$. The exponent of 0.54 is in line with the exponents for published heat transfer correlations for multijet impingement cooling, which typically show a range between 0.5 and 0.8 [21]. The achieved minimal thermal resistance of the 3-D printed 4 × 4 cooler is 0.16 cm^2·K/W for a flow rate of 1000 mL/min.

B. Hydraulic Analysis

Fig. 9(a) shows the comparison of the pressure drop for the two coolers on the level of the full cooler. In this section, the hydraulic results are extracted from the full-level CFD models in order to analyze the contribution of different components for the overall pressure drop. This total pressure drop is defined as the pressure difference between the inlet and the outlet tubes of the cooler, and includes the following contributions:

$$\Delta P_{\text{total}} = \Delta P_{\text{unit}} + \Delta P_{\text{inlet chamber}} + \Delta P_{\text{outlet chamber}}. \quad (3)$$

1) The pressure drop of the inlet chamber $\Delta P_{\text{inlet chamber}}$: This is the pressure difference between the cooler inlet tube and the inlet nozzle on the nozzle plate. The pressure at the inlet of the nozzle plate is defined as

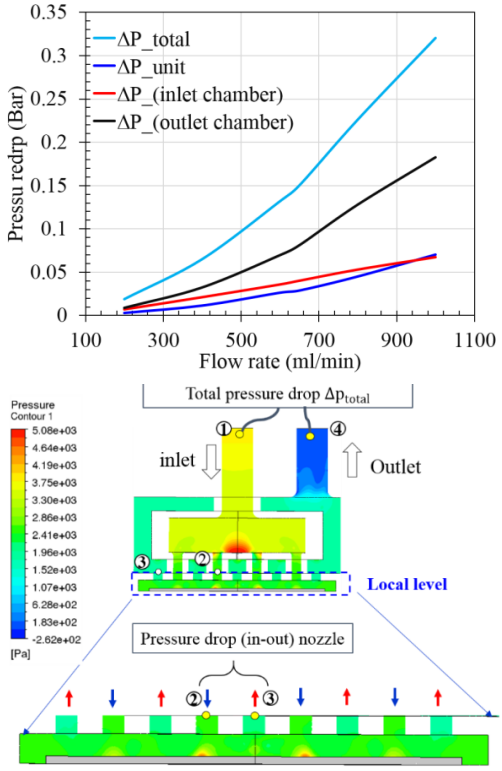

Fig. 18. CFD simulation results for the pressure drop analysis of 3-D printed cooler and the indications of the pressure defined positions. (Note: The curves in the figure are all simulation results from the CFD model.)

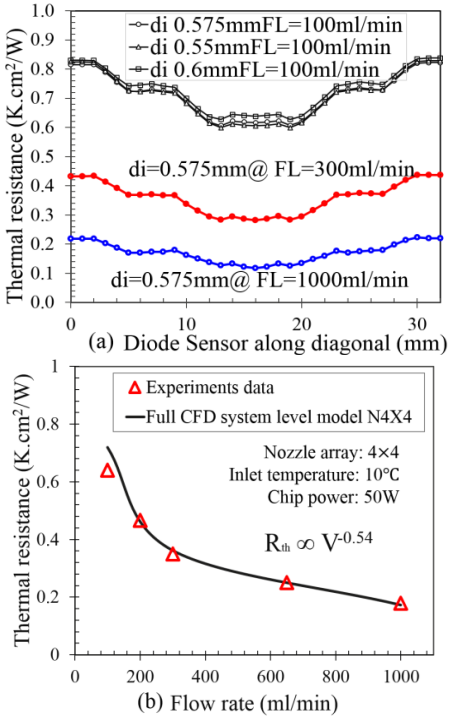

Fig. 19. System-level CFD modeling results of the 3-D printed 4×4 cooler. (a) Impact of the nozzle diameter on the thermal performance using CFD modeling. (b) Full-CFD model validation with experimental results.

the average pressure in the coolant at the beginning of the inlet nozzle for the 16 inlet nozzles. This pressure drop corresponds to the difference between the locations "1" and "2" shown in Fig. 17(b).

2) The pressure drop between inlet nozzle and outlet nozzle ΔP_{unit} in a cooling unit cell: This pressure drop includes the contributions from the inlet and outlet channels, the impingement region, and the wall jet region. This corresponds to the pressure drop between locations "2" and "3."
3) The pressure drop of the outlet chamber $\Delta P_{\text{outlet chamber}}$; between the nozzle outlet (3) and the cooler outlet tube (4), where the pressure at the nozzle outlet is defined as the average pressure of the 25 outlet nozzles.

The evolution of the total cooler pressure drop and different contributions are shown in Fig. 18, as a function of the total flow rate in the cooler. The cooler pressure drop and the pressure drop contributions all scale with the second power of the flow rate. It can be observed that the pressure drop in the outlet plenum is responsible for the major contribution to the total pressure, while the pressure drop contribution in the inlet plenum and the nozzle plate are considerably smaller. At the flow rate of 1000 mL/min, the pressure drop contribution of the outlet plenum amounts to 57%, while the inlet plenum and nozzle plate contributions to the pressure drop are 21% and 22%, respectively. The reason for the dominance of the outlet plenum contribution is the large pressure drop associated with the flow through narrow gaps between the cylinder of the inlet/outlet divider, shown in Fig. 5, and the collection of the outlet flow in a single outlet connector. The large difference is pressure drop associated with the local nozzle level, and the global cooler level in both plenums shows that improvement efforts to reduce the cooler pressure drop should be focused on distributor optimization for the inlet and outlet plenums rather than the nozzle level.

C. Experimental Model Validation

In this section, the full-cooler-level CFD simulations are updated with the measured nozzle diameter of 575 μm and the nozzle plate thickness of 550 μm, and the modeling results are validated by experimental data for different flow rates. Fig. 19(a) shows the modeling results of the chip temperature along the chip diagonal for different flow rates. For the flow rate of 100 mL/min, the impact of the nozzle diameter variation is also shown. This impact analysis shows that the 5% diameter variation for the fabrication only results in a reduction of the average temperature and the minimal temperature of 4.7% and 4.3% for the same flow rate, respectively. In Fig. 19(b), the average thermal resistance of the chip is compared for the modeling results and the measurement data as a function of the flow rate. It can be seen that the maximum error between the modeling result and experiments is 12% at 100 mL/min, while the difference reduces to 4% at the high flow rate of 1000 mL/min. In conclusion, the CFD model used in this paper is validated and shows good agreement with the experimental results.

V. Benchmarking Study

As shown in Fig. 20(a), in order to put the thermal performance and size of the 3-D printed cooler in perspective,

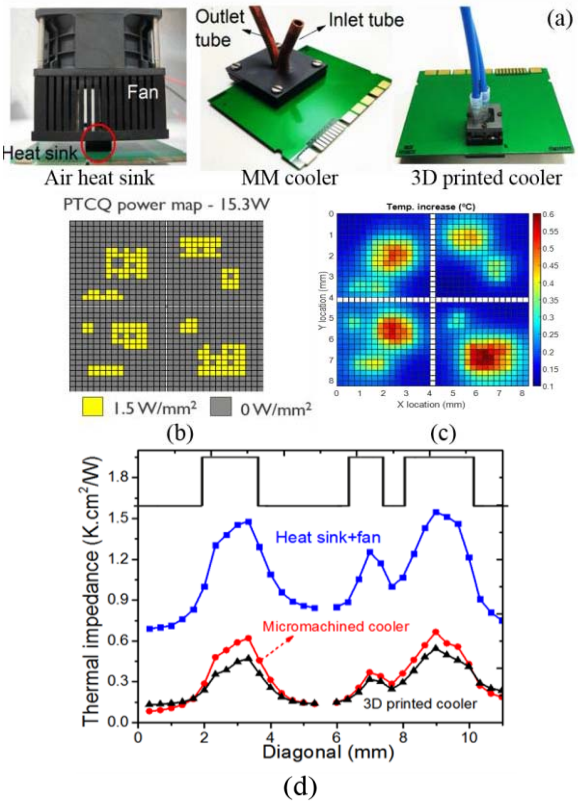

Fig. 20. Comparison of the measured chip temperature map for the heat sink, micromachined cooler, and the 3-D printed cooler. (a) Three demonstrators' comparison. (b) Defined PTCQ hot spots power map. (c) Measured temperature map with 3-D printed cooling. (d) Measured temperature profile comparison.

the measured chip temperature map is compared for a conventional heat sink–fan combination, the MM polymer liquid jet cooler [6] (600 mL/min) and the 3-D printed liquid jet cooler (600 mL/min) for a custom power dissipation map. As mentioned before, the cooler is part of a closed-flow loop system, and this comparison only considers the size of the cooler on the chip since the intention of the proposed cooler is to replace a bolt-on liquid cold plate in the existing infrastructure with the pump, tubing, and heat exchanger. It should be noted that the size of the additional parts in the closed loop is not considered here. The chosen power map with different hot spot sizes that is applied to the thermal test chip is shown in Fig. 20(b). The measured chip temperature increase map is shown in Fig. 20(c) for the case of the 3-D printed cooler. Fig. 20(d) shows the comparison of the temperature profiles along the chip diagonal for the three different coolers. The comparison shows that both liquid jet coolers achieve a 2.7× lower peak temperature difference and a 3.5× lower average temperature difference with respect to the inlet temperature compared to the conventional air cooling heat sink. The size of the coolers is, respectively, 8 mm × 8 mm, 46 mm × 46 mm, and 18 mm × 18 mm for the heat sink and fan combination, the MM cooler, and the 3-D printed cooler, respectively. This clearly shows that the 3-D cooler offers a huge reduction in the cooler size, matching the footprint of the chip package.

VI. Conclusion

In this paper, a chip-level 3-D printed microjet liquid impingement cooler containing 4 × 4 nozzle arrays with 575-μm nozzle diameter is demonstrated using the SLA 3-D printing technology. The experimental characterization shows a low thermal resistance of 0.16 cm^2·K/W for a flow rate of 1000 mL/min and a pressure drop of 0.3 bar and also good temperature uniformity. Moreover, the CFD modeling results show a good agreement with the measurements data, which are used for the cooler geometry optimization and thermal and hydraulic performance analyses. The printing quality and fabrication tolerance of 3-D printed cooler are assessed using different measurement methodologies. The printed impingement jet cooler exhibits lower pressure drop and allows the reduction of the cooler size compared to the MM cooler and conventional heat sink, which enables significant cost and performance improvements for cooling solutions of the high-performance applications. In summary, the 3-D printing can allow creating much more complex internal geometries with better hydraulic performance that is not feasible to create with conventional techniques.

References

[1] G. Van der Plas *et al.*, "Design issues and considerations for low-cost 3-D TSV IC technology," *IEEE J. Solid-State Circuits*, vol. 46, no. 1, pp. 293–307, Jan. 2011.

[2] T. Brunschwiler *et al.*, "Direct liquid jet-impingment cooling with micron-sized nozzle array and distributed return architecture," in *Proc. IEEE ITHERM*, May/Jun. 2006, pp. 196–203.

[3] G. Natarajan and R. J. Bezama, "Microjet cooler with distributed returns," *Heat Transf. Eng.*, vol. 28, nos. 8–9, pp. 779–787, 2007.

[4] T. Acikalin and C. Schroeder, "Direct liquid cooling of bare die packages using a microchannel cold plate," in *Proc. 14th Intersoc. Conf. Therm. Thermomech. Phenomena Electron. Syst.*, May 2014, pp. 673–679.

[5] K. Gould, S. Q. Cai, C. Neft, and A. Bhunia, "Liquid jet impingement cooling of a silicon carbide power conversion module for vehicle applications," *IEEE Trans. Power Electron.*, vol. 30, no. 6, pp. 2975–2984, Jun. 2015.

[6] T. Tiwei *et al.*, "High efficiency direct liquid jet impingement cooling of high power devices using a 3D-shaped polymer cooler," in *IEDM Tech. Dig.*, San Francisco, CA, USA, Dec. 2017, pp. 32.5.1–32.5.4.

[7] G. Aspar *et al.*, "3D printing as a new packaging approach for MEMS and electronic devices," in *Proc. IEEE 67th Electron. Compon. Technol. Conf. (ECTC)*, May/Jun. 2017, pp. 1071–1079.

[8] M. Craton, J. A. Byford, V. Gjokaj, J. Papapolymerou, and P. Chahal, "3D printed high frequency coaxial transmission line based circuits," in *Proc. IEEE 67th Electron. Compon. Technol. Conf. (ECTC)*, May/Jun. 2017, pp. 1080–1087.

[9] T. Tiedje, S. Lüngen, M. Schubert, M. Luniak, K. Nieweglowski, and K. Bock, "Will low-cost 3D additive manufactured packaging replace the fan-out wafer level packages?" in *Proc. IEEE 67th Electron. Compon. Technol. Conf. (ECTC)*, May/Jun. 2017, pp. 1065–1070.

[10] C. Bailey, S. Stoyanov, T. Tilford, and G. Tourloukis, "3D-printing and electronic packaging," in *Proc. Pan Pacific Microelectron. Symp. (Pan Pacific)*, Big Island, HI, USA, Jan. 2016, pp. 1–7.

[11] C. Bailey, S. Stoyanov, T. Tilford, and G. Tourloukis, "3D-printing and electronic packaging—Current status and future challenges," in *Proc. IEEE 18th Electron. Packag. Technol. Conf. (EPTC)*, Nov./Dec. 2016, pp. 1–4.

[12] M. Vaezi, H. Seitz, and S. Yang, "A review on 3D micro-additive manufacturing technologies," *Int. J. Adv. Manuf. Technol.*, vol. 67, nos. 5–8, pp. 1721–1754, 2013.

[13] B. Tehrani, R. Bahr, D. Revier, B. Cook, and M. Tentzeris, "The principles of 'smart' encapsulation: Using additive printing technology for the realization of intelligent application-specific packages for IoT, 5G, and automotive radar applications," in *Proc. IEEE 68th Electron. Compon. Technol. Conf. (ECTC)*, May/Jun. 2018, pp. 111–117.

[14] B. Goubault *et al.*, "A new microsystem packaging approach using 3D printing encapsulation process," in *Proc. IEEE 68th Electron. Compon. Technol. Conf. (ECTC)*, San Diego, CA, USA, May/Jun. 2018, pp. 118–124.
[15] E. M. Dede, S. N. Joshi, and F. Zhou, "Topology optimization, additive layer manufacturing, and experimental testing of an air-cooled heat sink," *J. Mech. Des.*, vol. 137, no. 11, pp. 111403-1–111403-9, 2015.
[16] F. F. Wang and E. Parker, "3D printed micro-channel heat sink design considerations," in *Proc. Int. Symp. 3D Power Electron. Integr. Manuf. (3D-PEIM)*, Raleigh, NC, USA, Jun. 2016, pp. 1–13.
[17] R. Jenkins, C. De Brún, R. Kempers, R. Lupoi, and A. J. Robinson, "Thermal-hydraulic performance of convective boiling jet array impingement," *J. Phys., Conf. Ser.*, vol. 745, no. 3, 2016, Art. no. 032120.
[18] A. J. Robinson, W. Tan, R. Kempers, J. Colenbrander, N. Bushnell, and R. Chen, "A new hybrid heat sink with impinging micro-jet arrays and microchannels fabricated using high volume additive manufacturing," in *Proc. 33rd Therm. Meas., Modeling Manage. Symp.*, Mar. 2017, pp. 179–186.
[19] B. P. Whelan, R. Kempers, and A. J. Robinson, "A liquid-based system for CPU cooling implementing a jet array impingement waterblock and a tube array remote heat exchanger," *Appl. Therm. Eng.*, vol. 39, pp. 86–94, Jun. 2012.
[20] H. Oprins *et al.*, "Experimental thermal characterization and thermal model validation of 3D packages using a programmable thermal test chip," in *Proc. IEEE 65th Electron. Compon. Technol. Conf. (ECTC)*, San Diego, CA, USA, May 2015, pp. 1134–1141.
[21] T. Wei *et al.*, "3D printed liquid jet impingement cooler: Demonstration, opportunities and challenges," in *Proc. IEEE 68th Electron. Compon. Technol. Conf. (ECTC)*, San Diego, CA, USA, May/Jun. 2018, pp. 2389–2396.
[22] T. Wei *et al.*, "High efficiency polymer based direct multi-jet impingement cooling solution for high power devices," *IEEE Trans. Power Electron.*, to be published.
[23] N. Zuckerman and N. Lior, "Jet impingement heat transfer: Physics, correlations, and numerical modeling," *Adv. Heat Transf.*, vol. 39, pp. 565–631, 2006.
[24] A. Khaled, S. Brand, M. Kögel, T. Appenroth, and I. De Wolf, "Investigating stress measurement capabilities of GHz scanning acoustic microscopy for 3D failure analysis," *Microelectron. Rel.*, vol. 64, pp. 336–340, Sep. 2016.

Tiwei Wei (M'17) was a Researcher Staff with Tsinghua University, Beijing, China, and also with The Hong Kong University of Science and Technology, Hong Kong, from 2011 until 2015, where he was responsible for the test vehicles design, process development and experimental characterization in 3-D system integration technologies related to 3-D/2.5-D integration, through silicon via (TSV), and through glass via (TGV). In 2015, he joined imec, Leuven, Belgium, where he conducted his Ph.D. research with developing thermal cooling solutions for high-performance systems. He is currently a Ph.D. Researcher with imec. He has authored over 13 publications including IEDM, ECTC, and EPTC, and one Outstanding Paper Award in ICEPT 2013. He holds nine Chinese national patents and one U.S. patent in the area of advanced packaging.

Herman Oprins (M'18) received the M.Sc. and Ph.D. degrees in mechanical engineering from KU Leuven, Leuven, Belgium.

In 2003, he joined imec, Leuven, where he was involved in modeling and experimental projects on thermal management of electronic packages. Since 2009, he has been a Senior Research Engineer with imec, where he is involved in the thermal experimental characterization, thermal modeling and management of 3-D-ICs, electronic packages, GaN transistors, photovoltaic modules, and microfluidics.

Vladimir Cherman (A'14) received the M.S. and Ph.D. degrees in electronic engineering from Saint Petersburg Electrotechnical University (LETI), Saint Petersburg, Russia, in 1994 and 1999, respectively.

From 1997 to 2000, he was an Electronics Engineer with Morion, Inc., Saint Petersburg. From 2000 to 2007, he was with the Ceramics Laboratory, Swiss Federal Institute of Technology Lausanne (EPFL), Lausanne, Switzerland, where he researched microwave properties of ferroelectric materials. Since 2007, he has been a Researcher with imec, Leuven, where he is involved in reliability studies of microelectromechanical systems devices and electronic packages.

Shoufeng Yang received the B.Eng. degree in mechanical engineering and the Ph.D. degree in materials science and engineering from Tsinghua University, Beijing, China, in 1994 and 1999, respectively.

He was a Chair Professor of additive manufacturing with the The University of Southampton, Southampton, U.K., from 2010 to 2016, a Senior Lecturer and Lecturer with the Queen Mary University of London, London, U.K., from 2000 to 2010, and a Post-Doctoral Researcher with Nanyang Technological University, Singapore, from 1999 to 2000. Since 2016, he has been a Professor of additive manufacturing with the Department of Mechanical Engineering, Production Engineering, Machine Design and Automation, Faculty of Engineering, KU Leuven, Leuven, Belgium.

Ingrid De Wolf (M'05–SM'10) received the Ph.D. degree in physics from KU Leuven, Leuven, Belgium.

In 1989, she joined imec, Leuven, where she was involved in the field of microelectronics reliability. From 1999 to 2014, she was the Head of the REMO Group, imec, where she was focused on reliability, test, and modeling. She is currently a Chief Scientist with imec and a Professor with the Department of Materials Engineering, KU Leuven. She has authored or coauthored several book chapters and more than 350 publications.

Eric Beyne (M'83–SM'17) received the master's degree in electrical engineering and the Ph.D. degree in applied sciences from KU Leuven, Leuven, Belgium, in 1983 and 1990, respectively.

Since 1986, he has been with imec, Leuven, where he has been involved in advanced packaging and interconnect technologies. He is currently a fellow with imec, where he is the Program Director of the 3-D System Integration Program.

Martine Baelmans received the Ph.D. degree in engineering from KU Leuven, Leuven, Belgium, in 1993.

She is currently a Professor with the Department of Mechanical Engineering, KU Leuven, where she leads the group on thermal-fluid engineering since 1996. She has authored or co-authored more than 200 papers in applications on fluid mechanics and heat transfer. Research topics are presently focusing on automated optimization in thermal design. Starting from dedicated component and system models, parameters, shapes, and topologies are improved. Applications range from liquid and two-phase cooling over thermal management in power electronics, power transformers, and energy systems.